Optical detection of symmetric and antisymmetric states in double quantum wells at room temperature

M. Marchewka,[1] E. M. Sheregii,[1] I. Tralle,[1] A. Marcelli,[2] M. Piccinini,[2] and J. Cebulski[1]
[1]*Institute of Physics, University of Rzeszów, Rejtana 16a, Rzeszów 35-959, Poland*
[2]*INFN-Laboratori Nazionali di Frascati, Via E. Fermi 40, I-00044 Frascati, Italy*
(Received 2 December 2008; revised manuscript received 2 July 2009; published 17 September 2009)

We studied the optical reflectivity of a specially grown double quantum well (DQW) structure characterized by a rectangular shape and a high electron density at room temperature. Assuming that the QWs depth is known, reflectivity spectra in the mid-IR range allow to carry out the precise measurements of the SAS-gap values (the energy gap between the symmetric and anti-symmetric states) and the absolute energies of both symmetric and antisymmetric electron states. The results of our experiments are in favor of the existence of the SAS splitting in the DQWs at room temperature. Here we have shown that the SAS gap increases proportionally to the subband quantum number and the optical electron transitions between symmetric and antisymmetric states belonging to different subbands are allowed. These results were used for interpretation of the beating effect in the Shubnikov-de Haas (SdH) oscillations at low temperatures (0.6 and 4.2 K). The approach to the calculation of the Landau-levels energies for DQW structures developed earlier [D. Ploch *et al.*, Phys. Rev. B **79**, 195434 (2009)] is used for the analysis and interpretation of the experimental data related to the beating effect. We also argue that in order to explain the beating effect in the SdH oscillations, one should introduce two different quasi-Fermi levels characterizing the two electron subsystems regarding symmetry properties of their wave functions, symmetric and antisymmetric ones. These states are not mixed neither by electron-electron interaction nor probably by electron-phonon interaction.

DOI: 10.1103/PhysRevB.80.125316 PACS number(s): 78.67.De

I. INTRODUCTION

Double quantum wells (DQWs) provide a convenient and unique test system of the electron-electron (e-e) interaction when electrons are confined inside the potentials originated by closely arranged bilayers. Besides the phenomena such as Bose condensation[1,2] or the Wigner crystallization[3,4] in DQW induced by a high magnetic field at ultralow temperatures, another interesting issue of such systems is still open, for instance, the possibility to determine the symmetric and antisymmetric electron states and measuring the so called SAS splitting or SAS gap (the magnitude of symmetric and antisymmetric states splitting in DQW) at normal conditions, e.g., at room temperature. These topics attracted considerable interest due to their relevance to the possible device applications and quantum computation.[5]

The optical phenomena such as photoluminescence and intersubband absorption play crucial role in the optical devices based on DQW structures such as infrared detectors,[6] photodetectors,[7] and quantum cascade lasers.[8] The detection of symmetric and antisymmetric electron states in DQWs by optical methods, e.g., by means of infrared transmission at room temperature (the energy distance between electron states actually is affected by several factors, such as the depth and width of QW and for a typical QW is about 0.1 eV, which corresponds approximately to the wavelength of $\lambda \approx 10$ μm) would be of significant interest, because this method is a direct one allowing to determine the SAS gap as well as the energies of the symmetric and antisymmetric states.

In this work we present the results of our study of the optical transitions between electron states in specially grown structure containing DQW characterized by a rectangular shape, high electron mobility and high electron density (see Refs. 9 and 10). We will show that in these DQWs the SAS gap (Δ_{SAS}) increases with the quantum number of a subband increasing and that the selection rules do not impose limitations on the optical transitions between symmetric and antisymmetric states belonging to the different subbands.

The magnitudes of SAS gap determined by this way, further on is used for the interpretation of beating effect in the Shubnikov-de Haas (SdH) oscillations observed at low temperatures in the external magnetic field perpendicular to the two-dimensional electron gas (2DEG) layers (that is, $B_{\|}$ component was equal zero in our experiments). There is no doubt that the beating effect in SdH oscillation is the result of the nonzero SAS gap in zero magnetic field. As it will be seen further, in order to account for the beating effect occurring in SdH oscillations in the DQWs with the matched density of states, it is necessary to introduce two different quasi-Fermi levels, one for the symmetric and another one for antisymmetric electron subsystem, respectively.[11] In our previous works[9–11] the values of energy of states in a rectangular QWs, E_i has been calculated by means of a numerical procedure which took into account a finite height of a barrier, for example, as it is shown in Ref. 12. The SAS gap in zero magnetic field (Δ^S_{SAS}) (the superscript s is for screening, since we took into account also the screening effect) was introduced as the fit parameter for the calculation of Landau-levels (LLs) energies, in order to interpret the experimental data on SdH oscillations. Therefore, the direct measurement of the magnitude of SAS gap independently by optical experiments is important for correct interpretation of the magnetotransport data obtained at low temperatures.

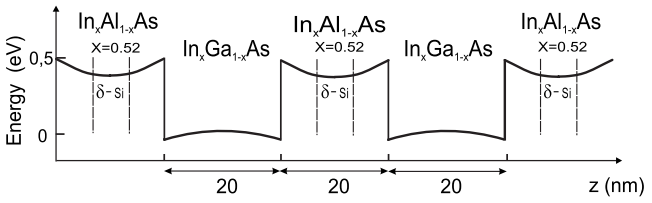

FIG. 1. The profile of the conduction-band edges of the 2506 DQW structure.

II. EXPERIMENT AND RESULTS

A. Description of the DQW structure

DQWs based on InGaAs/InAlAs/InP structures were produced at the Institute of Electronic Material Technology in Warsaw by means of the low-pressure metal organic vapor phase epitaxy on semi-insulating (100) InP:Fe substrates (see Refs. 9 and 10 for details). The investigated structure (2506) consists of two InGaAs QWs of about 20 nm thickness each, and three InAlAs barriers.

In each barrier there was the donor δ-doping layer (see Fig. 1). The quasirectangular shape of these QWs is shown in Fig. 1 together with that of the conduction-band profile of the whole structure. In order to reconstruct this shape, we used calculations carried out for the $In_{0.52}Al_{0.48}As/In_{0.65}Ga_{0.35}As$ QW.[13] An accurate study of the electron transport of this structure has been performed in Refs. 14 and 15 and the parameters obtained for the 2DEG in the channels of the structure are summarized in Table I. Here we have to stress that due to smooth interfaces,[9] the investigated QWs have a quasirectangular shape. Although the thickness of the barrier between QWs seems large, nevertheless strong interaction between layers occurs, as it is shown in Ref. 11.

The electron density in the 2D layers of DQWs is very high and the number of carriers in the two QWs (total width of the QWs is about 40 nm) is three orders of magnitude higher than in a semi-insulating InP substrate of 0.5 mm thickness. As a consequence, the contribution of the 2DEG to optical experimental data in the mid-IR range is dominant. For these optical experiments in the mid-IR range, as well as for magnetotransport measurements, the samples of 2×0.4 mm^2 prepared by photolithography were used [see Fig. 3(a)].

B. Optical experiment in the mid-IR region

Reflectivity spectra in the mid-IR range were collected at the SINBAD (Synchrotron Infrared Beamline at DAΦNE) of the Laboratori Nazionali di Frascati, INFN (Italy), an instrument designed to work at IR wavelengths ranging from about 1 to 2000 μm (5–10000 cm^{-1}). A BRUKER Equinox 55 interferometer and a BRUKER Hyperion 3000 IR microscope with a spot of 5 μm were used to collect reflectivity spectra with the resolution of 1.5 cm^{-1} in 19 different locations chosen on a line on top of the sample at a distance of 0.1 mm each [see Fig. 3(a)]. The layout of the optical experiment is shown in Fig. 2. For these reflectivity experiments we have to take into account that wavelengths in the mid-IR range, i.e., 4–20 μm, are considerably larger than the thickness of the structure investigated, i.e., the sum of the thicknesses of two QWs and three barriers, which is about 100 nm.

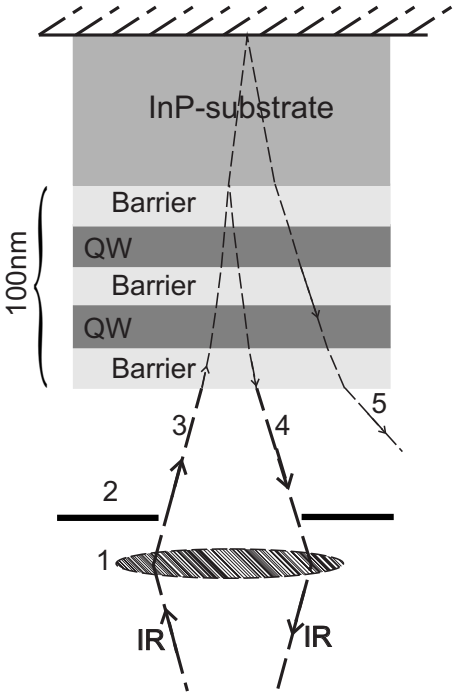

FIG. 2. Layout of the reflectivity experiment with the IR Microscope: 1 is Ge lens, 2 is diaphragm, 3 is the incident beam, 4 is the reflected beam from the substrate, and 5 is the beam reflected from the metal holder of the sample.

Assuming that the IR radiation is mainly reflected by the surface of the substrate of semi-insulationg InP (see Fig. 2) we expect that the reflected signal contains information about absorption in the DQWs.[16] It is because of the optical setup of the microscope (the incident beams are not parallel), interference effects generated by multiple reflections due to the internal plane-parallel layered structure are averaged out and are not detected in the resonance spectra.[17]

TABLE I. Parameters of the InGaAs/InAlAs DQW structure.

Sample	Concentration of InAs in the channels (%)	Thickness of the channels (nm)	QW profile	The electron mobility $\times 10^5$ cm^2/(Vs)	The 2D electron density $\times 10^{12}$ cm^{-2}
2506	65	20	smooth interface	1.2[a]	4.1[b]

[a]On the Landau levels in the magnetic field 2–5 T at the temperature 4.2 K.
[b]At 4.2 K.

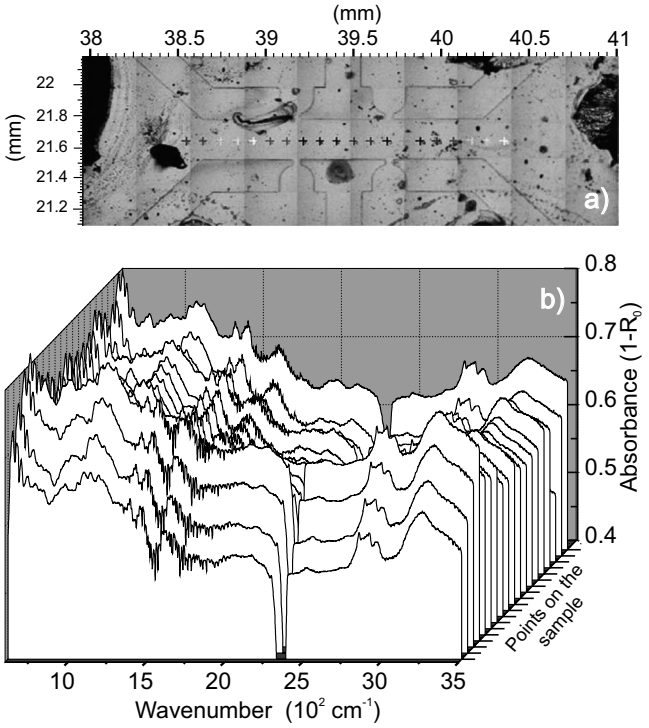

FIG. 3. (a) Image of the sample with the experimental points where reflectivity data were collected. (b) The 19 experimental absorbance spectra of the the structure at 2506.

Due to absorption, a DQW structure decreases the reflectivity $R(\omega)$, and we have to consider the difference $1-R(\omega)$ (i.e., the absorbance) in order to determine the absorption lines associated with optical transitions between DQW electronic states. Absorbance data are shown in Fig. 3(b) for each experiment, while in Fig. 4 we show the average of the 19 absorbance curves measured at different locations.

If one looks at these IR spectra, one can easily notice the wide-structured absorption band, where the first subband starts at 600 cm^{-1} and last one starts at 3600 cm^{-1}. In these experiments the relative reflectivity of the DQW structure

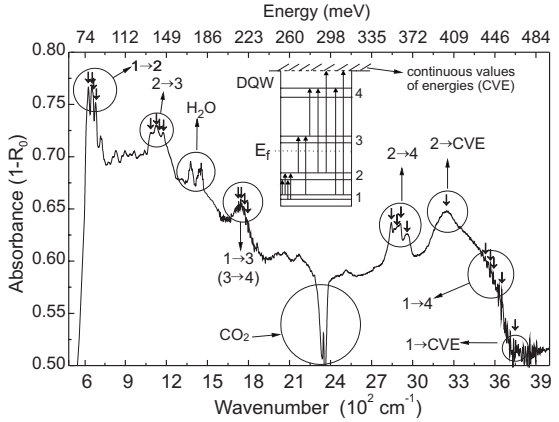

FIG. 4. The average spectra of the 19 spectra curves, shown in Fig. 3(b). In the inset is the scheme of the DQW electronic states of the one of the well (the second one is identical) showing the electron transmission between DQW levels.

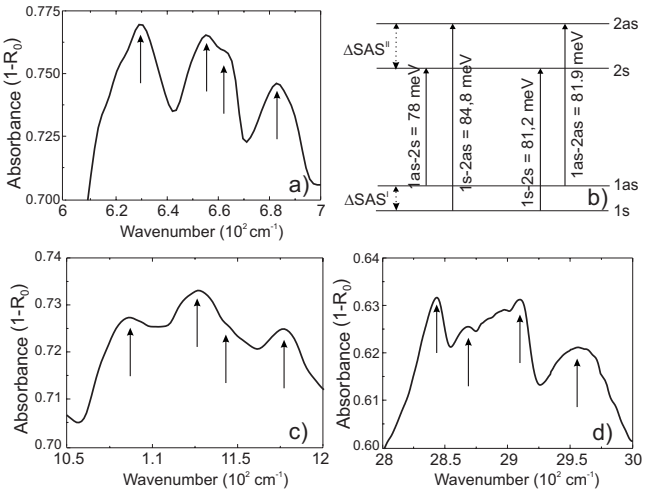

FIG. 5. (a) Three spectral subbunds extracted from spectral curve in Fig. 4 corresponding to optical transitions among electronic states; (a) spectral subband corresponding to the electron transitions between first and second energetic subbands in DQWs; (b) four possible electron transitions (black arrow) between two energetic subbands: 1as→2s; 1s→2as; 1s→2s; and 1as→2as; (c) spectral subband corresponding to the electron transitions between second and third energetic subbands; and (d) spectral subband corresponding to the electron transitions between second and fourth energetic subbands.

was measured using gold mirror as the reference, in order to exclude the influence of an air gap between the objective of the IR mirror and the sample. As a result, the strong absorption lines of CO_2 and H_2O due to air gap are cancelled. However, small contributions to the spectra at 2350 and 1350 cm^{-1} are probably due to an incomplete suppression of the CO_2 and H_2O lines, respectively.[17]

C. Results

The wide absorption band observed in the averaged absorbance spectral curve shown in Fig. 4 consists of several subbands whose frequency corresponds to the electron transitions between the electron states. The energies of these states can be estimated by the extrapolation of the LL energies at zero magnetic field. We used these calculated values of the LL energies to interpret magnetotransport phenomena observed at low and ultralow temperatures in the same DQW (see Ref. 11). The frequency of the optical lines marked in Fig. 4 as $1\rightarrow 2$, $2\rightarrow 3$, $2\rightarrow 4$, and $2\rightarrow$CVE, are in agreement with the calculated values of the symmetric and antisymmetric states energies[11] (deviations will be discussed later). All transitions indicated in Fig. 4 enable us to determine directly, with high precision, the electron state energies and the corresponding SAS gaps at room temperature with the resolution of 1.5 cm^{-1} (0.19 meV).

If now one looks at the three optical subbands marked as 1–2, 2–3, and 2–4 in Fig. 4 separately, as shown in Fig. 5 at a zoom, then it is seen that each of these three subbands consists of four lines (the center line split in two components). Four optical lines may correspond to the four possible electron transitions between the initial and final states (each

TABLE II. The values of Δ^S_{SAS} and energies of symmetric E^s_i and antisymmetric E^{as}_i states in successive energetic subband obtained from optical experiment.

	First subband	Second subband	Third subband	Fourth subband
Δ^S_{SAS} (meV)	3.1 ± 0.2	3.9 ± 0.3	6.6 ± 0.2	9.4 ± 0.4
E^s_i (meV)	12.0	93.1	232.2	448.9
E^{as}_i (meV)	15.1	97.0	239.0	458.4

of them are split into symmetric and antisymmetric ones). The difference between the first (which corresponds to the smallest transition energy) and the fourth transitions (corresponding to the largest transition energy) in each subband corresponds to the sum of the two SAS splitting.

Figure 5(a) illustrates the structure of the first spectral subband consisting of four lines which are in between 600–700 cm^{-1}. The first line at 629 cm^{-1} (78 meV) is responsible for the transition from the antisymmetric state of the first subband (1as) to the symmetric state in the second subband (2s). The fourth line [the last from the right in Fig. 5(a)] at 684 cm^{-1} (84.8 meV) corresponds to the electron transition from the symmetric state of the first subband (1s) to the antisymmetric state of the second subband (2as). The sum of SAS gaps for these two subbands is

$$E_{1s} - E_{2as} = \Delta^{I}_{SAS} + \Delta^{II}_{SAS} = 6.8 \text{ meV}. \quad (1)$$

Beside these two transitions another two transitions, $1as \rightarrow 2as$ and $1s \rightarrow 2s$, occur. A scheme of the transitions between the first and the second energy subbands of the DQW is shown in Fig. 5(b). The wave-numbers values of the corresponding lines enable to determine the corresponding energies of photons which are 81.2 and 81.9 meV, respectively. This provides the additional equations for calculating the SAS gap. The details of the calculations are summarized in Appendix A.

This method allows to obtain the SAS-gap values for four energy subbands of the DQW; they are presented in Table II. The values of the state energies can be estimated by means of spectral subband marked as (CVEs) in Fig. 4, which corresponds to the electron transitions from the second energy subband to the lowest state of the CVE spectrum. Consider now the 2-CVE peak in Fig. 4. The position of the spectral line shows that the corresponding transition energy is equal to 405 meV $\pm$ 4 meV and the peak should include two transitions, $2s \rightarrow CVE$ and $2as \rightarrow CVE$, whereas we observe only a single line with a negligible distortion on the low-energy side. Probably, the spatial distribution of the density of states in the vicinity of the lowest state of the CVE blurs the absorption edge and induces a broadening of the peaks due to the transitions $2s \rightarrow CVE$ and $2as \rightarrow CVE$. As a result, only one maximum is observed and the position of peak due to $2s(as) \rightarrow CVE$ transition allows to determine experimentally the energies of all subbands of DQW, using the following simple relations:

$$E^{s(as)}_i - E^{s(as)}_{i-1} = \tilde{\nu}_i, \quad (2)$$

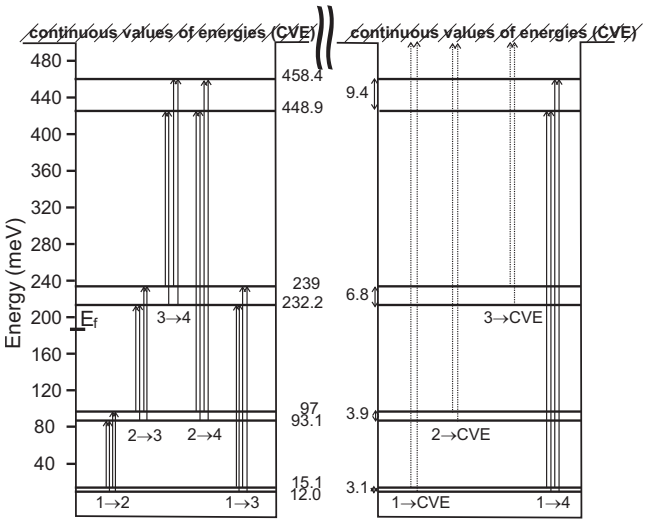

FIG. 6. The scheme of DQW with the electron transition between electron states and with calculated the values of energy levels and SAS gap for all subbands.

where the $\tilde{\nu}_i$ is the center of the corresponding spectral line. If we assume, in agreement with the calculations carried out in Ref. 13, that the depths of the two QWs are about 500 meV, we can measure the position of subbands with respect to the bottom of QWs. Energies of each subbands (together with the SAS gaps), are summarized in Table II. A scheme of the energy states in DQWs and the possible electron optical transitions are shown in Fig. 6.

It can be seen that the Δ^s_{SAS} increases when the quantum number of subband increases. This experimental result is in agreement with the theoretical predictions[18] and explains why the SAS gap for each energy subband in a DQW increases, being smaller for the first subband and greater for the last one. Indeed, it is quite obvious that (i) higher states are more extended, so their overlap between the two wells increases; (ii) the height of the barrier decreases for electrons which occupy higher energy level.

Comparing the data of the state energies for the 2506 DQW obtained in our previous work[11] (using, as it is mentioned in the introduction, numerical calculations of the energy of states in the rectangular quantum well with finite depth) with values obtained directly from optical measurements in this work, we find that differences are about 18%. It means that the model of rectangular QW does not reflect in all details features of real DQWs.

III. MAGNETOTRANSPORT AT LOW TEMPERATURES

It was noticed in the introduction that existence of SAS gap (Δ^S_{SAS}) at zero magnetic field is the origin of the beating effect of the SdH oscillations observed for DQW 2506 at low temperatures. The values of the Δ^S_{SAS} determined independently enable to perform a correct interpretation of the SdH beating effect.

A. Beating of the Shubnikov-de Haas oscillations

The magnetotransport measurements were performed by means of a superconducting magnet, which gives the possi-

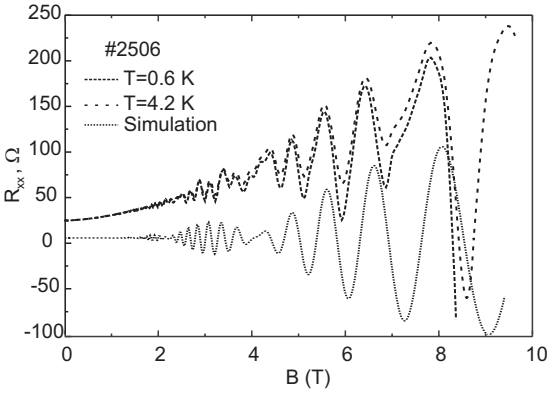

FIG. 7. The SdH oscillations at 0.6 and 4.2K together with the theoretical curve of SdH oscillations according to the method described in text.

bility to obtain magnetic fields up to 11 T. The sample was mounted in the anticryostat which allows to change the temperature from 0.4 to 300 K.[19] The external gate voltage was not applied because this field destroys the symmetry of the DQWs profiles. The values of Hall $[U_{xy}(B)]$ as well as longitudinal $U_{xx}(B)$ voltage were recorded for the two opposite directions of magnetic and electric fields. Therefore, eight records (for magnetic field once going up and then going down) were made and averaged at each single measurement for the transverse magnetoresistance $R_{xx}(B)$ and Hall resistance $R_{xy}(B)$ at given temperatures.

The records of magnetoresistance for two different temperatures are presented in Fig. 7. The two upper curves in Fig. 7 present the experimental records for 0.6 and 4.2 K and the lower one represents the results of the transverse magnetoresistance calculation performed according to the method described in detail below.

It can be unequivocally stated that the SdH oscillations undergo the beating effect which was observed in our experiments for the temperatures ranging from 0.6 to 8 K. The Fourier analysis of the observed SdH oscillation data is presented in Fig. 8. The two main components of the SdH oscillation that split the main maximum at about value of B_f=40 T are clearly seen in Fig. 8.

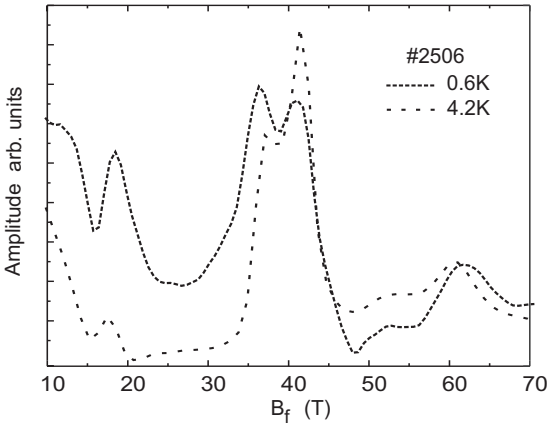

FIG. 8. The SdH-oscillations' Fourier transform plotted versus $B_f=[\Delta(1/B)]^{-1}$.

On the other hand, our earlier experiments with the structures containing a single quantum well,[9,10] did not show a beating effect of SdH oscillations which could be attributed to spin splitting. Therefore we can conclude, that another kind of electron state splitting also takes place and it exists in zero magnetic field also. This state's splitting is the splitting of symmetric and antisymmetric states in the DQWs. In order to reveal this most important effect, we have used the following method of the experimental SdH curve simulation. The starting point for further analysis is the next expression, which is well known in the theory of SdH oscillations[20]

$$\frac{\Delta\rho}{\rho_0}=\sum_{l=1}^{\infty}\frac{5}{2}\left(\frac{lP}{2B}\right)^{1/2}\frac{\beta Tm'\cos(l\pi\nu)}{\sinh(\beta Tm'/B)}$$
$$\times\exp(-l\beta T_D m'/B)\cos 2\pi(l/PB-1/8-l\gamma). \quad (3)$$

This formula takes into account the nonparabolicity of the conduction band as well as spin splitting. Here $\Delta\rho$ is the deviation of ρ from background resistivity, ρ_0 is zero-field resistivity, B is the transverse magnetic field, T is the temperature, $\beta=2\pi^2k_Bm_0/\hbar e$, is the Dingle temperature, $P=\hbar e/E_fm^*$ stands for the SdH period. The fitting procedure was based on adding only two Fourier harmonics of nearly equal frequencies. According to what was mentioned above, formula (3) can be simplified and reduced to two entries of the Fourier series only. As a result we have

$$\Delta\rho_{xx}^1=\exp\left(-\frac{\gamma_1}{B}\right)\cos\left[2\times(\omega_1-kB)\times\frac{\pi}{B}\right] \quad (4)$$

and

$$\Delta\rho_{xx}^2=\exp\left(-\frac{\gamma_2}{B}\right)\cos\left[2\times(\omega_2+kB)\times\frac{\pi}{B}\right], \quad (5)$$

where γ_1 and γ_2 are the coefficients which are equivalent to $R\beta T_Dm'$ in Eq. (3), ω_1, ω_2 are the cyclotron frequencies for two subsystems of Landau levels. The kB term is included into the argument of cosine in Eqs. (4) and (5) in order to have an additional degree of freedom to get better agreement between the experimental and calculated curves.

The result of the calculations are shown in Fig. 7 for the sample 2506. The parameters used in the calculations, were chosen to be: γ_1=8.8, γ_2=8, ω_1=34.9, ω_2=40.27, and k=0.095, where ω_1 and ω_2 are the values of frequencies taken from Fourier analysis for the second dominating peak split into two. In this way we have obtained two oscillation components for each SdH curve, the sum of these two components are presented on Fig. 7 as the lower curve. Using only these two split frequencies obtain from Fourier analysis it is possible to fit the experimental curve with very good accuracy. The two components of the SdH oscillations should be interpreted using the LL energy calculations which should be carried out for the symmetric and antisymmetric states separately, by means of the best-fit procedure.

B. Calculation of Landau-level energy

The general scheme of the LL energies calculations in DQWs was elaborated in our previous work[15] where the

screening of the exchange interaction in DQWs was taken into account according to Ref. 21. In our approach an external magnetic field was considered to be applied perpendicular to the planes of QWs. The electron's behavior was described by the Schrödinger equation which includes the DQW potential, as well as the self-consistent Hartree potentials.[21]

This approach in our particular case of symmetric $In_{0.65}Ga_{0.35}As/In_{0.52}Al_{0.48}As$ DQW structure (2506) with rectangular QWs, enables to calculate the Landau-level energies according to the expressions

$$\frac{(E-E_\perp)(E_g+E+E_\perp)}{E_g}=E_i, \tag{6}$$

$$E_\perp=-\frac{E_g}{2}-\frac{E_g}{2}\times\sqrt{1+\frac{4\mu_B B}{E_g}\left[f_1\frac{m_0}{m_c^*}\left(n+\frac{1}{2}\right)\pm\frac{1}{2}g_0^* f_2\right]}, \tag{7}$$

where

$$f_1=\frac{E_g+\frac{2}{3}\Delta}{E_\perp+E_g+\frac{2}{3}\Delta}$$

$$f_2=\frac{(E_g+\Delta)\left(E_\perp+E_g+\frac{2}{3}\Delta\right)}{\left(E_g+\frac{2}{3}\Delta\right)(E_\perp+E_g+\Delta)} \tag{8}$$

$$E'=E\pm(\Delta_{\mathrm{SAS}}^S+kB), \tag{9}$$

where E_g is the energy gap (between the top of valence band and the edge of conduction band) and Δ is spin-orbital splitting, m_0 is the electron mass in a vacuum, m_c^* is the effective electron mass corresponding to the edge of the conduction band, μ_B is the Bohr magneton, $n=1,2,3,\ldots$ stands for Landau levels, $i=1,2,3,\ldots$ is the number of subbands, E_i are the values of the subband energies presented in Table II, $E_\perp$ is the LLs energy for bulk semiconductor, E is the LLs energy in single QW and E' is the unknown LLs energy for symmetric and antisymmetric states in DQWs. The Δ_{SAS}^S is also shown in Table II for each subband and, as was mentioned above, it is the energy gap determined by the overlapping of the wave functions, which is diminished by the screening at zero magnetic field as it follows from Refs. 11 and 21: $\Delta_t=(\Delta_{\mathrm{SAS}}-K_0)+kB\equiv\Delta_{\mathrm{SAS}}^S+kB$. Thus, the SAS gap is proportional to the magnetic field B according to the experimental data of Ref. 22 and Eq. (9) and it deliver an explanation of the beating effect in SdH oscillations. The coefficient k is to be considered as the same fitting parameter as in Eqs. (4) and (5).

The calculations of LL's energies were performed according to Eqs. (6)–(9) for the sample 2506 with the same band-structure parameters as in Ref. 11 but with values of Δ_{SAS}^S and E_i taken from Table II. The results of our calculations for the sample 2506 are shown in Fig. 9 (for the symmetric states) and in Fig. 10 for the antisymmetric states. The calculated energies are plotted versus magnetic field for two subbands ($i=1,2$). Usually the Fermi-level (FL) position is determined by LL's and FL crossings corresponding to the maxima of two components of SdH oscillations, acquired by simulation of the beating effect. It is worth mentioning that,

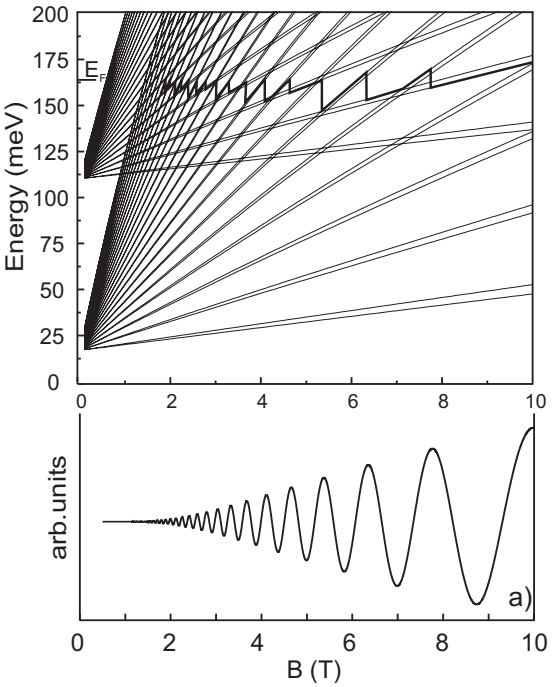

FIG. 9. This figure represents the best fit of the Fermi-level energy corresponding to symmetric part of the SdH oscillations in case of the structure 2506

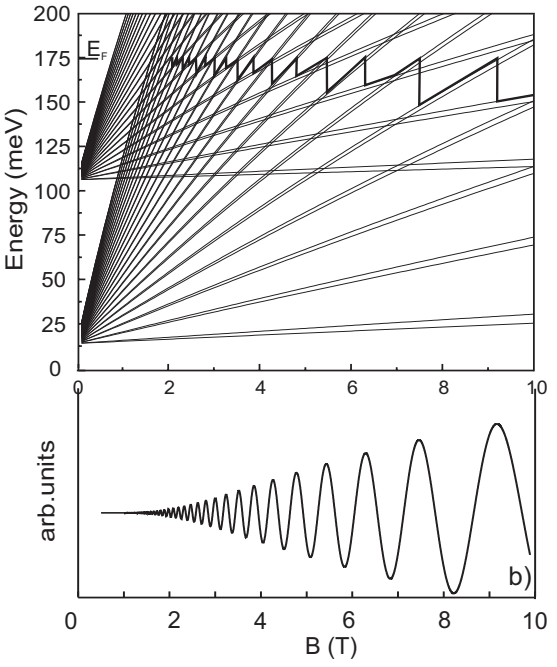

FIG. 10. This figure represents the best fit of the Fermi-level energy corresponding to antisymmetric part of the SdH oscillations, in case of the structure 2506.

as it is seen in the Figs. 9 and 10, the FL positions are perfectly well fitted to the oscillation curves and are unique, since they correspond to the regularly spaced crossings of LL's, equidistant with respect to the inverse magnetic field. The FL displacement up or down, destroys this regularity immediately, due to the superposition of the two space-quantized subbands.

We should admit that we could not achieve satisfactory agreement between our experimental data and the theoretical predictions about the SdH oscillation peaks positions, if we tried to use the single Fermi level common for both types of the states, symmetric and antisymmetric. As it is clearly seen in Figs. 9 and 10, the Fermi levels for two oscillation components are different, and the difference is equal to 12 meV.

The obtained values of the FL energies give us the possibility to estimate the density of carriers for the investigated structure. This value is 3.8×10^{12} cm^{-2} which is in a good agreement with the data obtained by the slope of $R_{xy}(B)$ curve in a small magnetic field and is presented in Table I.

IV. DISCUSSION

Our experimental data forced us to introduce the concept of two quasi-Fermi levels, by means of which two electron subsystems can be characterized. These two subsystems are the electrons belonging to two different types of states, symmetric and antisymmetric. One can encounter the concept of quasi-Fermi levels in different contexts for instance, in semiconductor physics. The quasi-Fermi levels for electrons and holes very often are used; quasi-Fermi levels for the electron states with $\mathbf{k}_{+x}$ and $\mathbf{k}_{-x}$ ($\mathbf{k}$ are for the electron wave vectors along say, $+x$ and $-x$) are introduced to explain the peculiarities of IQHE,[23,24] and so on. Generally speaking this concept simply means, that one can treat two subsystems as weakly interacting and having their own rate of establishing the equilibrium state. Therefore, our next step is to argue that indeed, we could interpret our data, introducing the two quasi-Fermi levels which characterize two separate electron subsystems.

A. Electron-electron interaction for the two subsystems: Symmetric and antisymmetric states

Suppose now that the 2DEG in the DQW structure under consideration is off the thermodynamic equilibrium state and the deviations from the equilibrium are small enough. Obviously, these deviations are caused by the current which flows through the structure. Then the electron distribution functions, one of which corresponds to the symmetric state $f^{(a)}$ and the other to antisymmetric one $f^{(b)}$, can be represented as follows:

$$f^{(a,b)} = f_0^{(a,b)}(\vec{k}) + \delta f^{(a,b)},(\vec{k}) \tag{10}$$

where

$$\delta f^{(a)}(\vec{k}) = \delta_{\vec{k}\vec{k}_0'}\delta f^{(a)}(\vec{k}_0'),$$

$$\delta f^{(b)}(\vec{k}) = \delta_{\vec{k}\vec{k}_0'}\delta f^{(b)}(\vec{k}_0'). \tag{11}$$

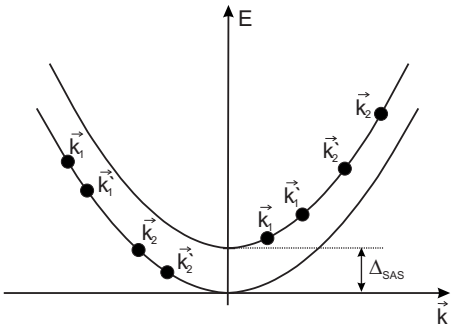

FIG. 11. Diagram, representing the electron-electron scattering in case of two subbands, symmetric and antisymmetric.

Here the superscript a stands for the symmetric and b for the antisymmetric states (see Appendix B) where the wave functions for this states are considered). They denote the electrons belonging to subsystem a by means of Ψ_a, and belonging to subsystem b as Ψ_b and define the rate of establishing the equilibrium state in each subsystem as

$$\frac{1}{\tau^{(a,b)}(\vec{k})} = \sum_{\vec{k}'} \{W_{\vec{k}\to\vec{k}'}^{(a,b)}[1 - f_0^{(a,b)}(\vec{k}')] + f_0^{(a,b)}(\vec{k}')W_{\vec{k}'\to\vec{k}}^{(a,b)}\}$$

$$= \sum_{\vec{k}'} W_{\vec{k}\to\vec{k}'}^{(a,b)} \frac{1 - f_0^{(a,b)}(\vec{k}')}{1 - f_0^{(a,b)}(\vec{k})}, \tag{12}$$

where $W_{\vec{k}\to\vec{k}'(\vec{k}'\to\vec{k})}^{(a,b)}$ are the probabilities for the electrons belonging to the subsystem a or b to be scattered from the state k to the state k' and vice versa (see Fig. 11). These probabilities are determined by the following formula:

$$W_{i\to f}^{(a,b)} = \frac{2\pi}{\hbar}|\langle\Psi_f^{(a,b)}|\hat{V}|\Psi_i^{(a,b)}\rangle^2|\delta(E_i^{(a,b)} - E_f^{(a,b)}), \tag{13}$$

where $|\Psi_i^{(a,b)}\rangle$ and $|\Psi_f^{(a,b)}\rangle$ are the initial and final states, $E_i^{(a,b)}$ and $E_f^{(a,b)}$ are their energies, respectively, and $\hat{V}$ is the operator, corresponding to the perturbation responsible for the transition. It is well known that sometimes mainly the electron-electron (e-e) collisions lead to establishing the equilibrium states within an electron gas in a semiconductor at low temperatures.[25] It means that whatever the initial distribution function is, the final distribution can be described by a displaced Fermi distribution function. However, for establishing such distribution, an important condition has to be satisfied: e-e collisions should be more frequent than the electron-phonon (e-ph) collisions. In other words, $\tau_{\text{e-e}} \ll \tau_{\text{p-ph}}$, where $\tau_{\text{e-e}}$ and $\tau_{\text{e-ph}}$ are the e-e and e-ph scattering times, respectively. Since in our experiments we dealt with the degenerate electron gas and the temperatures at which our experiments were carried out, were low, we can suppose the last condition was fulfilled. Now in order to calculate $\tau_{\text{e-e}} = \tau^{(a,b)}$ for the two subsystems, we have to calculate $W_{\vec{k}\to\vec{k}'}^{(a,b)}$, the corresponding transition probabilities. Therefore, we should analyze the probabilities for two electrons to transit from the states $(l_1k_1, l_2k_2)^{(a,b)}$ to the states $(l_1'k_1', l_2'k_2')^{(a,b)}$ where (l_1, l_1', l_2, l_2') stand for the quantum numbers, other then k.

Notice that the subscripts 1,2 stand for the electrons 1 and 2 in a pair, while the superscripts (a,b) are to distinguish symmetric and antisymmetric states of the electrons in DQW structure. Then

$$W^{(a,b)}_{(a,b)\to(1'2')} = \frac{2\pi}{\hbar}|M^{(a,b)}_{(1,2)\to(1',2')}|^2 \times \delta(\epsilon_1^{(a,b)} + \epsilon_2^{(a,b)} - \epsilon_1'^{(a,b)} - \epsilon_2'^{(a,b)}). \quad (14)$$

Here we introduced the following notations $l_1 k_1 \equiv 1$, $l_1' k_1' \equiv 1'$ etc; $\epsilon_1^{(a,b)}$, $\epsilon_2^{(a,b)}$, $\epsilon_1'^{(a,b)}$, $\epsilon_2'^{(a,b)}$, are the electron energies in the initial and final states, respectively. It is necessary to calculate the matrix elements $M^{(a,b)}_{(1,2)\to(1',2')}$ in Eq. (14) to show the different rates of establishing of the quasiequilibrium states in two subsystems. The calculation of two elements $M^{(a)}_{(1,2)\to(1',2')}$ and $M^{(b)}_{(1,2)\to(1',2')}$ is carried out in Appendix B.

On inspecting Eqs. (B5) and (B6), even without evaluating these integrals, one can easily see that $M^{(a)}_{(1,2)\to(1',2')} \neq M^{(b)}_{(1,2)\to(1',2')}$ and hence, the same is true for $\tau^{(a,b)}_{e-e}$: $\tau^{(a)}_{e-e} \neq \tau^{(b)}_{e-e}$. That is, the rates of establishing a quasiequilibrium state under electron-electron scattering in the two subsystems, corresponding to the symmetric and antisymmetric subbands, are different.

The same arguments are also valid if we consider the e-ph interaction. Moreover in the case of electron-phonon interaction the formulas analogous to Eqs. (B5) and (B6) are even simpler, because in this case the initial as well the final electron states are one-particle states, but not two-particles states, as in the case of electron-electron scattering. Nevertheless one can state that both $\tau^{(a,b)}_{e\text{-}e}$ and $\tau^{(a,b)}_{e\text{-}ph}$ in two subsystems corresponding to the symmetric and antisymmetric states, are different: $\tau^{a}_{e\text{-}e} \neq \tau^{b}_{e\text{-}e}$; $\tau^{a}_{e\text{-}ph} \neq \tau^{b}_{e\text{-}ph}$.

The only thing which also has to be proven, is that these two subsystems are weakly interacting. To this end let us consider the transition matrix element $M^{(c)}_{(1,2)\to(1',2')}$, where (1,2) stands for the initial state which includes the symmetric state Ψ_i^a, and $(1',2')$ stands for the final state which includes the antisymmetric state, Ψ_f^b. Then, under the integral sign in Eq. (B6) one should have the product of two functions $\varphi_a(z_1)$, $\varphi_b(z_1)$, one is even and the other one is odd. Notice also, that U^{ee} is an even function of its variables. Hence, $M^{(c)}_{(1,2)\to(1',2')}$ should be very nearly to zero due to the parity selection rule, and it means that the electron-electron scattering does not mix the states of different parities.

B. Electron-phonon interaction

Of course, electron-phonon interaction can and usually does mix them. Yet we can argue that in our magnetotransport experiments even at the temperatures of about 77–80 K the acoustic as well as optical phonons do not mix these symmetric and antisymmetric states. Indeed, let us consider at first the kinematics of electron scattering by optical phonons. It is clear that the symmetric and antisymmetric states inside the subband would be mixed by such a scattering process, if the next equality were held: $\Delta^S_{SAS} = \pm\hbar\omega_{LO}$, where the upper sign refers to the emission of LO phonons while lower sign refers to their absorption. Note that this relation is nothing else but the energy conservation law for this particular case. However, as our experiments show, even for the magnetic field of about 25 T the Δ^S_{SAS} is not greater than 15 meV, while the energy of LO phonon is about 30 meV, and hence, such scattering process does not occur and the optical phonons do not mix the symmetric and antisymmetric states inside one subband. In the case of the intersubband transitions with the participation of the LO phonons the next resonance condition must be fulfilled: $E_{is(as)n^{\pm}} - E_{i's(as)n'^{\pm}} = \hbar\omega_{LO}$, which means that the magnetophonon resonance (see Ref. 15) takes place. The last transitions could mix the symmetric and antisymmetric states but they are essential at high magnetic fields (above 10 T).[15] Thus, we could expect that if the magnetophonon resonance condition is not fulfilled, the symmetric and antisymmetric states in the DQWs are not mixed and the whole electron system consists of two subsystems characterized by two different quasi-Fermi levels.

Proceed now to the acoustic phonons and consider the kinematics of electron scattering by acoustic phonons, the energy conservation law now reads: $\Delta^S_{SAS} = \pm\hbar v_s q$, where v_s stands for the sound velocity and q for the acoustic-phonon quasimomentum. Since in magnetotransport experiments the main contribution to the current is due to electrons whose energies ϵ are close to the Fermi energy, when some of the Landau levels cross the Fermi level, we can assume that $|\epsilon - \epsilon_F| \ll \epsilon_F$, $\epsilon \approx \epsilon_F$. Then the initial as well as the final states of the electron are on the energy surface which is very close to the Fermi surface and hence, $q = |k - k'| \leq k_F$, where k and k' are the initial and final electron quasimomenta, while k_F is the Fermi quasimomentum. Following the Ref. 26, we introduce the parameter, which can be considered as a kind of measure of the nonelasticity of electron-phonon scattering and define it as the number N_s of scattering events needed for the considerable change of electron energy. It our particular case it can be defined as

$$N_s \cong (2N_q + 1)\frac{|\epsilon - \epsilon_F|}{\Delta^S_{SAS}}, \quad (15)$$

where N_q is the occupation number of the corresponding phonon mode

$$N_q = \left[\exp\left(\frac{\hbar\omega_q}{k_B T}\right) - 1\right]^{-1} \quad (16)$$

Expanding the exponent in the last formula into the power series and taking into account that $|\epsilon - \epsilon_F| \propto k_B T$, we get the next expression for N_s

$$N_s = \frac{(2k_B T + \hbar\omega_q)k_B T}{\Delta^S_{SAS}\hbar\omega_q} = \frac{(2k_B T + \hbar\omega_q)k_B T}{\Delta^S_{SAS}\hbar v_s q}. \quad (17)$$

Assuming $q \propto q_T = k_B T/\hbar v_s$, where q_T is the quasimomentum of thermal acoustic phonons, taking for sound velocity the value $v_s = 5\times10^5$ cm/s, for $\Delta^S_{SAS} = 15$ meV and $T = 80$ K, we obtain for N_s a value greater than 10. It means that the electron undergoes many collisions with acoustic phonons until it makes the transition between the two states, corresponding to Δ^S_{SAS}. It means that the time which is

needed for such a transition is long enough and can be estimated to be about tens of nanoseconds, while the time flight across the structure is about a few ps.

C. Two quasi-Fermi levels

As a result first, the electron transport in such structure can be considered as ballistic with respect to the scattering by acoustic phonons and second, the quasiequilibrium state in each of the subsystems corresponding to the symmetric and antisymmetric states is established by electron-electron scattering. That is why we strongly believe that the two electron subsystems, symmetric and antisymmetric, in the case of current flow and lack of thermal equilibrium can be characterized by two quasi-Fermi levels, because, first, the main mechanism of electron relaxation, namely, the electron-electron scattering, does not mix the states of different parities and second, the equilibrium between generation and relaxation processes is established at different levels due to the current which flows in the system.

This situation is not unique: a very similar situation arises in spin injection from a ferromagnetic metal to diffusive semiconductor.[27] It is assumed that the rate of scattering events without spin flips of spin-up ($\uparrow$) and spin-down ($\downarrow$) electrons is much larger than the spin-flip rate. This implies that under nonequilibrium conditions two electrochemical potentials $\mu_\uparrow$ and $\mu_\downarrow$ may be defined at any point and they need not be equal (see Ref. 27).

Extrapolation allows us to assume that two electron subsystems in DQW structure, belonging to symmetric and antisymmetric states, are characterized by two different quasi-Fermi levels even at room temperature, which means that these two subsystems can be distinguished in electron transport measurements. The last one is very important for possible applications in quantum circuits.

V. SUMMARY

The optical reflectivity of the InGaAs/InAlAs-DQW structure has been measured at room temperature with a IR Microscope at 19 different space locations on the sample surface. Reflectivity data then were averaged using 19 spectra. The absorbance curve for the sample obtained in this way is characterized by three subbands, each consisting of four lines corresponding to four optical electron transitions between two energy states. These energy states correspond to even and odd states of coupled wells (we call them symmetric and antisymmetric throughout the text of the paper). The energy values of these three spectral bands enable us to calculate directly the energy values E_i and magnitudes of the SAS gap in the DQWs. The performed experiments allow to claim that: the SAS gap (Δ^S_{SAS}) at zero magnetic field increases as the quantum number of the subband increases; the selection rules do not forbid the optical transitions between symmetric and antisymmetric states if they belong to different subbands; at low temperatures the SAS gap is the origin of the beating effect in SdH oscillations and in order to account for the experimental results, it is needed to introduce two different quasi-Fermi levels, one for symmetric and another one for antisymmetric states; in our experiments SAS gap in DQWs is clearly seen at room temperature and in our opinion, it means that even at room temperature the system in question can be considered as consisting of two subsystems each of them characterized by two different quasi-Fermi levels. One can hope that such systems composed of two weakly interacting subsystems, could be used in quantum information applications.

ACKNOWLEDGMENTS

Authors are greatly indebted to M. von Ortenberg for invaluable discussions. This work was partly supported by the EU Foundation, the TARI Contract No. HPRI-CT-1999-00088.

APPENDIX A

To calculate the SAS gap for each energy subband, we need the two following equations:

$$\Delta^{\mathrm{I}}_{\mathrm{SAS}} = \begin{cases} E_{1s\to 2s} - E_{1as\to 2s} = 3.3 \ \mathrm{meV} \\ E_{1s\to 2as} - E_{1as\to 2as} = 2.9 \ \mathrm{meV} \end{cases} \tag{A1}$$

for the first energy subband and

$$\Delta^{\mathrm{II}}_{\mathrm{SAS}} = \begin{cases} E_{1s\to 2as} - E_{1s\to 2s} = 3.6 \ \mathrm{meV} \\ E_{1as\to 2as} - E_{1as\to 2s} = 3.9 \ \mathrm{meV} \end{cases} \tag{A2}$$

for the second one [in Eqs. (A1) the symbols $E_{1s\to 2s}$, $E_{1as\to 2s},\ldots,E_{1as\to 2s}$ are for the transitions energies determined by the positions of a spectral lines in Fig. 5(a), the scheme of this transitions as well as their energies are shown in Fig. 5(b)].

As we can see, the SAS-gap values obtained by means of different spectral lines are in good agreement (with an uncertainty of 8%). It is possible also to calculate energies of the states and the SAS gaps for all energy subbands in our DQWs structure using equations analogous to Eqs. (A1). For example, the electron transitions from the second to the third energy subband [the coresponding spectral lines are shown in Fig. 5(c)] enable us to calculate the SAS gap for the second energy subband

$$\Delta^{\mathrm{II}}_{\mathrm{SAS}} = \begin{cases} E_{2s\to 3s} - E_{2as\to 3s} = 4.2 \ \mathrm{meV} \\ E_{2s\to 3as} - E_{2as\to 3as} = 3.9 \ \mathrm{meV} \end{cases} \tag{A3}$$

while to calculate the $\Delta^{\mathrm{III}}_{\mathrm{SAS}}$ we used the same spectral lines [Fig. 5(c)]

$$\Delta^{\mathrm{III}}_{\mathrm{SAS}} = \begin{cases} E_{2s\to 3as} - E_{2s\to 3s} = 6.5 \ \mathrm{meV} \\ E_{2as\to 3as} - E_{2as\to 3s} = 6.8 \ \mathrm{meV} \end{cases}. \tag{A4}$$

Using the transitions between the second and fourth subbands [corresponding spectral lines are shown in Fig. 5(c)], one can obtain SAS gap for the fourth subband as well as that for the second one

$$\Delta^{\mathrm{II}}_{\mathrm{SAS}} = \begin{cases} E_{2s\to 4s} - E_{2as\to 4s} = 3.4 \ \mathrm{meV} \\ E_{2s\to 4as} - E_{2as\to 4as} = 4.1 \ \mathrm{meV} \end{cases} \tag{A5}$$

$$\Delta_{\mathrm{SAS}}^{\mathrm{IV}} = \begin{cases} E_{2s\to 4as} - E_{2s\to 4s} = 9.7 \text{ meV} \\ E_{2as\to 4as} - E_{2as\to 4s} = 9.0 \text{ meV} \end{cases}. \quad \text{(A6)}$$

The averaged values of SAS gaps are collected in Table II.

APPENDIX B

The Hamiltonian, which describes the electron moving in the potential like that of Fig. 1, is invariant under space coordinate inversion $z \to -z$ and hence, its eigenfunctions are double degenerate. However, due to the tunneling effect this degeneracy is removed and the lowest energy state in each quantum well becomes split into two, bounding and antibounding states represented by even and odd functions, respectively. We termed these states also as symmetric and antisymmetric ones. Then the eigenfunctions are of the form

$$\Psi_{a(b)} = \frac{1}{\sqrt{L_x}} \exp(ik_x x)\chi_m(y)\varphi_{a(b)}(z). \quad \text{(B1)}$$

In the last expression k_x is the wave vector along x axis, $\chi_m(y)$ is the wave function corresponding to the mth Landau level, L_x is the structure length along x axis, $\varphi_{a(b)}(z)$ stands for the antisymmetric (symmetric) state corresponding to the symmetric structure of the Fig. 1.

Two electrons interacting in the e-e scattering are indistinguishable and hence, the two electron states (1,2) and $(1',2')$, before and after scattering should be described by the Hartree-Fock determinants as follows:

$$\psi_1(\vec{r}_1)\psi_2(\vec{r}_2) = \frac{1}{\sqrt{2}}[\psi_1(\vec{r}_1)\psi_2(\vec{r}_2) - \psi_1(\vec{r}_2)\psi_2(\vec{r}_1)]. \quad \text{(B2)}$$

In order to calculate the matrix elements entering the expressions for $W^{(a,b)}_{\vec{k}\to\vec{k}'(\vec{k}'\to\vec{k})}$ in Eq. (14) using the last expression and Eq. (B1), one should substitute $\varphi_1(\vec{r}_1)$ and $\varphi_2(\vec{r}_2)$, $(i,j=1,2)$ by the next functions

$$\begin{aligned} \psi_{jb}(\vec{r}_i) &= \frac{1}{\sqrt{L_x}} \exp(ik_{jx}x_i)\chi_{mj}(y_i)\varphi_b(z_i) \\ &= \frac{1}{\sqrt{L_x}} \varphi_{\vec{k}j}(x_i)\chi_{mj}(y_i)\varphi_b(z_i), \\ \psi_{ja}(\vec{r}_i) &= \frac{1}{\sqrt{L_x}} \exp(ik_{jx}x_i)\chi_{mj}(y_i)\varphi_a(z_i) \\ &= \frac{1}{\sqrt{L_x}} \varphi_{\vec{k}j}(x_i)\chi_{mj}(y_i)\varphi_a(z_i), \end{aligned} \quad \text{(B3)}$$

where $\varphi_a(z_i)$ and $\varphi_b(z_i)$ correspond to symmetric and antisymmetric states, respectively. Here in the last expressions $k_j \equiv k_{jx}$ is the wave vector corresponding to the electron movement along x axis perpendicular to z axis. Introducing the Fourier transform of the screened Coulomb potential as

$$U^{ee}(r) = \int \frac{d^3q}{(2\Pi)^3} U_q^{ee} \exp(i\vec{q}\vec{r})d\vec{q} \quad \text{(B4)}$$

the corresponding matrix elements can be written down as follows:

$$\begin{aligned} M^{(a)}_{(1,2)\to(1',2')} = &\frac{1}{\sqrt{2L_x}} \int dV_1 \int dV_2 \varphi^*_{\vec{k}'1}(x_1)\chi^*_{m'1}(y_1) \\ &\times \varphi^*_b(z_1)\varphi^*_{\vec{k}'2}(x_2)\chi^*_{m'2}(y_2)\varphi^*_b(z_2)U^{ee}\varphi_{\vec{k}1}(x_1) \\ &\times \chi_{m1}(y_1)\varphi_b(z_1)\varphi_{\vec{k}2}(x_2)\chi_{m2}(y_2)\varphi_b(z_2) \\ &- \frac{1}{\sqrt{2L_x}} \int dV_1 \int dV_2 \varphi^*_{\vec{k}'1}(x_1)\chi^*_{m'1}(y_1) \\ &\times \varphi^*_b(z_1)\varphi^*_{\vec{k}'2}(x_2)\chi^*_{m'2}(y_2)\varphi^*_b(z_2)U^{ee}\varphi_{\vec{k}2}(x_1) \\ &\times \chi_{m2}(y_1)\varphi_b(z_1)\varphi_{\vec{k}1}(x_2)\chi_{m1}(y_2)\varphi_b(z_2), \end{aligned} \quad \text{(B5)}$$

$$\begin{aligned} M^{(b)}_{(1,2)\to(1',2')} = &\frac{1}{\sqrt{2L_x}} \int dV_1 \int dV_2 \varphi^*_{\vec{k}'1}(x_1)\chi^*_{m'1}(y_1)\varphi^*_a(z_1) \\ &\times \varphi^*_{\vec{k}'2}(x_2)\chi^*_{m'2}(y_2)\varphi^*_a(z_2)U^{ee}\varphi_{\vec{k}1}(x_1) \\ &\times \chi_{m1}(y_1)\varphi_a(z_1)\varphi_{\vec{k}2}(x_2)\chi_{m2}(y_2)\varphi_a(z_2) \\ &- \frac{1}{\sqrt{2L_x}} \int dV_1 \int dV_2 \varphi^*_{\vec{k}'1}(x_1)\chi^*_{m'1} \\ &\times (y_1)\varphi^*_a(z_1)\varphi^*_{\vec{k}'2}(x_2)\chi^*_{m'2}(y_2)\varphi^*_a(z_2)U^{ee} \\ &\times \varphi_{\vec{k}2}(x_1)\chi_{m2}(y_1)\varphi_a(z_1)\varphi_{\vec{k}1}(x_2)\chi_{m1}(y_2)\varphi_a(z_2), \end{aligned} \quad \text{(B6)}$$

where $U^{(ee)}_{q_\perp}$ is the two-dimensional Fourier transform of the screened Coulomb potential, $q_\perp = (q_x, q_y)$, $r_\perp = \sqrt{(y_1-y_2)^2+(z_1-z_2)^2}$. Note that regardless of the form of screening to occur, the corresponding potential $U^{ee}(r)$, $r = \sqrt{(x_1-x_2)^2+(y_1-y_2)^2+(z_1-z_2)^2}$ is an even function of its variables.

[1] V. Pellegrini, A. Pinczuk, B. S. Dennis, A. S. Plaut, L. N. Pfeiffer, and K. W. West, Phys. Rev. Lett. **78**, 310 (1997).

[2] J. P. Eisenstein and A. H. MacDonald, Nature (London) **432**, 691 (2004).

[3] R. M. Lewis, P. D. Ye, L. W. Engel, D. C. Tsui, L. N. Pfeiffer, and K. W. West, Phys. Rev. Lett. **89**, 136804 (2002).

[4] R. M. Lewis, Y. P. Chen, L. W. Engel, D. C. Tsui, L. N. Pfeiffer, and K. W. West, Phys. Rev. B **71** 081301(R) (2005).

[5] N. E. Bonesteel, L. Hormozi, G. Zikos, and S. H. Simon, Phys. Rev. Lett. **95**, 140503 (2005).

[6] J. Dai, M. E. Raikh, and T. V. Shahbazyan, Physica E (Amsterdam) **34**, 311 (2006).
[7] E. Ozturk and I. Sokmen, Superlattices Microstruct. **41**, 36 (2007).
[8] *Intersubband Transitions in Quantum Wells: Physics and Device Application*, edited by H. C. Liu and F. Capasso (Academic, San Diego, 2000), Vol. I.
[9] G. Tomaka, E. M. Sheregii, T. Kakol, W. Strupinski, A. Jasik, and R. Jakiela, Phys. Status Solidi A **195**, 127 (2003).
[10] G. Tomaka, E. M. Sheregii, T. Kakol, W. Strupinski, R. Jakiela, A. Kolek, A. Stadler, and K. Mleczko, Cryst. Res. Technol. **38**, 407 (2003).
[11] M. Marchewka, E. M. Sheregii, I. Tralle, G. Tomaka, D. Ploch, W. Strupiski, A. Jasik, R. Jakiela, A. Kolek, A. Stadle, K. Mleczko, and D. Zak, Physica E (Amsterdam) **40**, 894 (2008).
[12] L. D. Landau and L. M. Lifszitz, *Quantum Mechanics: Non-Relativistic Theory* (Elsevier Science, Oxford, 1977).
[13] W. Zawadzki and P. Pfeffer, *Proceedings of the 10th International Conference on Narrow Gap Semiconductors and Related Small Energy Phenomena, Physics and Applications*, IPAP Conference Series Vol. 2 (Japan, 2001), p. 219.
[14] M. Marchewka, E. M. Sheregii, I. Tralle, G. Tomaka, and D. Ploch, Int. J. Mod. Phys. B **21**, 1511 (2007).
[15] D. Ploch, E. M. Sheregii, M. Marchewka, M. Wozny, and G. Tomaka, Phys. Rev. B **79**, 195434 (2009).
[16] J. D. E. McIntyre and D. E. Aspens, Surf. Sci. **24**, 417 (1971).
[17] The strong absorption line caused by the phonons of InP at 150–200 cm^{-1} can be omitted in the consideration, because it is far from the region of interest (600–3000 cm^{-1}). Absorption lines due to impurities, which are located in the region of interest, are too weak and we do not take them into account. In our experiments almost all optical paths pass through a vacuum chamber, the only exception is a small air gap between the sample and microscope objective. That is why the H_2O- and CO_2-strong absorption lines should be taken into account.
[18] G. Bastard, *Wave Mechanics Applied to Semiconductor Heterostructures* (Halsted, NewYork, 1988).
[19] The measurements at the temperature below of the 4.2 K were performed at the Rzeszow University of Technology.
[20] D. G. Seiler and A. E. Stephens, in *Landau Level Spectroscopy*, Modern Problems in Condensed Matter Science Vol. 27.2, edited by G. Landwehr and E. I. Rashba, (North-Holland, Amsterdam, 1991), pp. 1035–1137.
[21] D. Huang and M. O. Manasreh, Phys. Rev. B **54**, 2044 (1996).
[22] K. M. Brown, N. Turner, J. T. Nicholls, E. H. Linfield, M. Pepper, D. A. Ritchie, and G. A. C. Jones, Phys. Rev. B **50**, 15465 (1994).
[23] J. H. Davies, *The Physics of Low-Dimensional Semiconductors* (Cambridge University Press, Cambridge, 1997).
[24] S. Datta, *Electronic Transport in Mesoscopic System* (Cambridge University Press, Cambridge, 1999).
[25] P. C. van Son, H. van Kempen, and P. Wyder, Phys. Rev. Lett. **58**, 2271 (1987); G. Schmidt, D. Ferrand, L. W. Molenkamp, A. T. Filip, and B. J. van Wees, Phys. Rev. B **62**, R4790 (2000); S. D. Ganichev, E. L. Ivchenko, V. V. Bel'kov, S. A. Tarasenko, M. Sollinger, D. Weiss, W. Wegscheider, and W. Prettl, Nature (London) **417**, 153 (2002).
[26] V. Gantmacher and Y. Levinson, *Carrier Scattering in Metals and Semiconductors* (North-Holland, New York, 1987).
[27] T. Valet and A. Fert, Phys. Rev. B **48**, 7099 (1993).